

Note on the transfer matrix measurement of a TESLA cavity (preliminary results)

P. Piot¹ and Y.-E. Sun²

¹Fermi National Accelerator Laboratory, Batavia IL 60510, USA

²University of Chicago, Chicago IL 60637, USA

December 30, 2004

Abstract

In the present note we report on our preliminary experimental investigations of the first order trace space transfer matrix, of the TESLA cavity installed at FNPL. These preliminary data, are compared with analytical and numerical models.

1 Theoretical background

The transfer matrix of an rf-section was derived by Chambers in the late 60's [1]. The model considers the motion of an ultra-relativistic beam in a standing wave structure operating on the π -mode. Chambers' model has been generalized to the case of an arbitrary (including higher space harmonic) accelerating structure in Reference [2]. References [1] and [2] however assumes the end-regions field of the cavity only provide a focusing kick and no acceleration – this is the so-called “hard edge” model. In reality, there is no open boundary condition allowing such an hard edge model: e.g. the axial electric field has fringes that extend in the beam pipe on each sides of the structure. Therefore we expect some correction of the analytical model derived in [1, 2]. The main results of Reference [1] is that the trace space transfer matrix of a cylindrical symmetric standing wave rf-structure, operating on the π -mode, is given by:

$$R = \begin{bmatrix} \cos \alpha - \sqrt{2} \cos \varphi \sin \alpha & \sqrt{8} \frac{\gamma_i}{\gamma'} \cos \varphi \sin \alpha \\ -\frac{\gamma'}{\gamma_f} \left(\frac{\sin \varphi}{\sqrt{2}} + \frac{1}{\sqrt{8} \cos \varphi} \right) \sin \alpha & \frac{\gamma_i}{\gamma_f} \left(\cos \alpha + \sqrt{2} \cos \varphi \sin \alpha \right) \end{bmatrix}, \quad (1)$$

where γ_i, γ_f are the initial and final Lorentz factors, $\alpha = \frac{1}{\sqrt{8} \cos \varphi} \log \frac{\gamma_f}{\gamma_i}$ and γ' is the normalized accelerating gradient. In virtue of adiabatic damping the determinant of R is $|R| = \gamma_i/\gamma_f$. There are several limitations of this model worth discussing in our case. Firstly, the incoming beam is not ultra-relativistic ($\gamma_i \simeq 8$), and there can be some phase slippage between the electric field and the beam. Such an effect has been studied in Reference [3] and does not appear to be significant in the range of injection phase we explored in our experiment ($\varphi \in [-40, 40]$ deg). Secondly a numerical integration of the transverse equation of motion reveals, compared to the Chamber formulation, that the matrix is not a symmetric function of the injection phase φ [4]. For completeness, we compare the transfer matrix elements computed from equation 1, with the result of the numerical integration of the transverse equation of motion in an rf structure, and a tracking simulation using elegant in a sine-like axial field (i.e. a field of the form $E_z(z) = E_0 \sin(kz)$); see Fig. 1. In Figure 2, we compare the transfer matrix resulting from numerical simulations for the exact axial-field of

the TESLA-type cavity and for sine-like field. The point is made that the Chamber model is only approximate in our regime and the exact transfer matrix need to be obtained from numerical simulations.

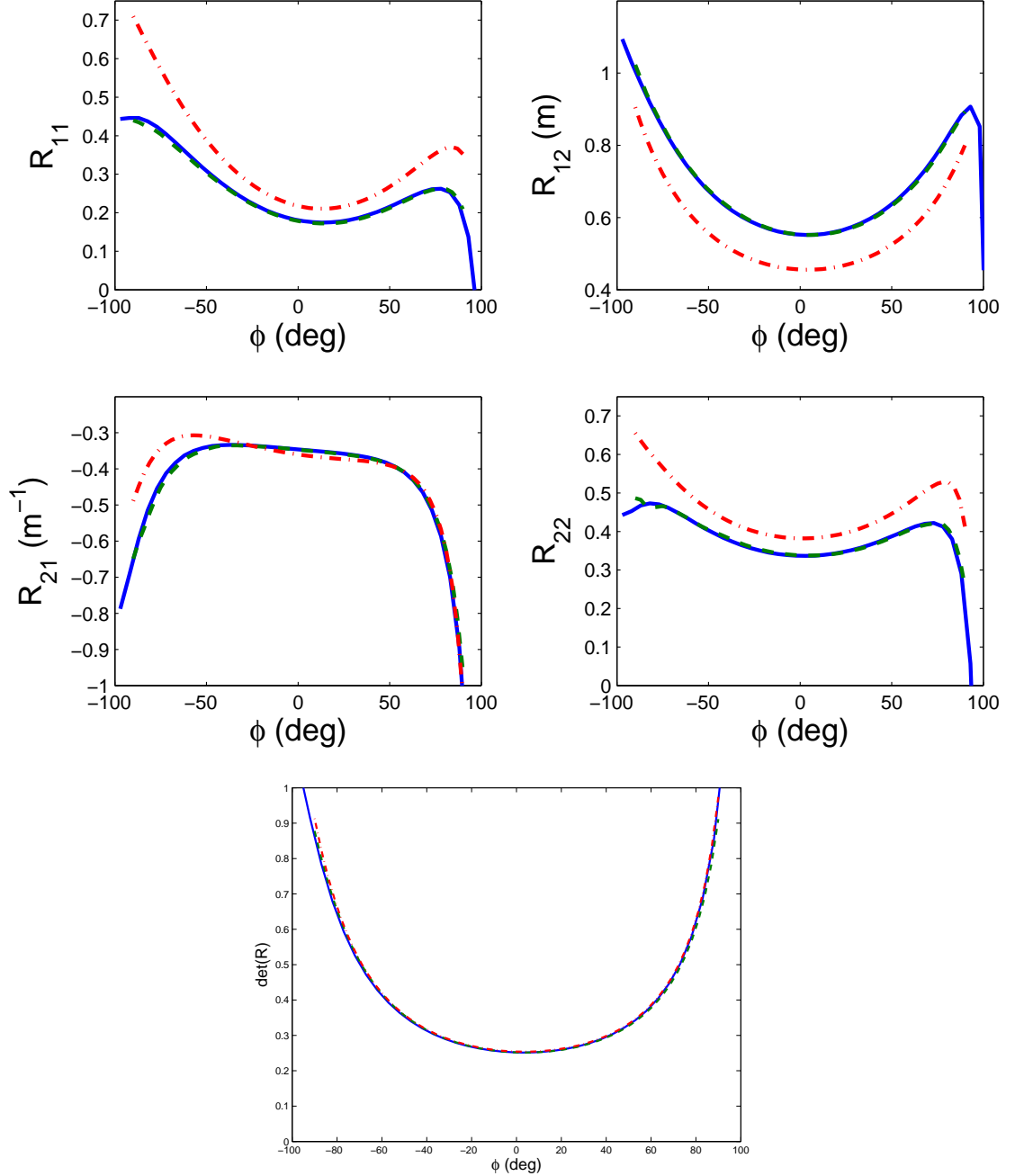


Figure 1: Transfer matrix elements and determinant dependence on the injection phase. The different curves correspond to ELEGANT (blue solid lines), ASTRA simulations (dashed green lines), taking $E(z) = E_0 \sin(kz)$. Elegant simulation with the exact axial field in a TESLA cavity is also shown (red dashed lines). The parameters are $\gamma' m_e c^2 \simeq 12$ MeV/m, $\gamma_i = 8$.

In the simulations the transfer matrix is computed by simply tracking two macroparticles of

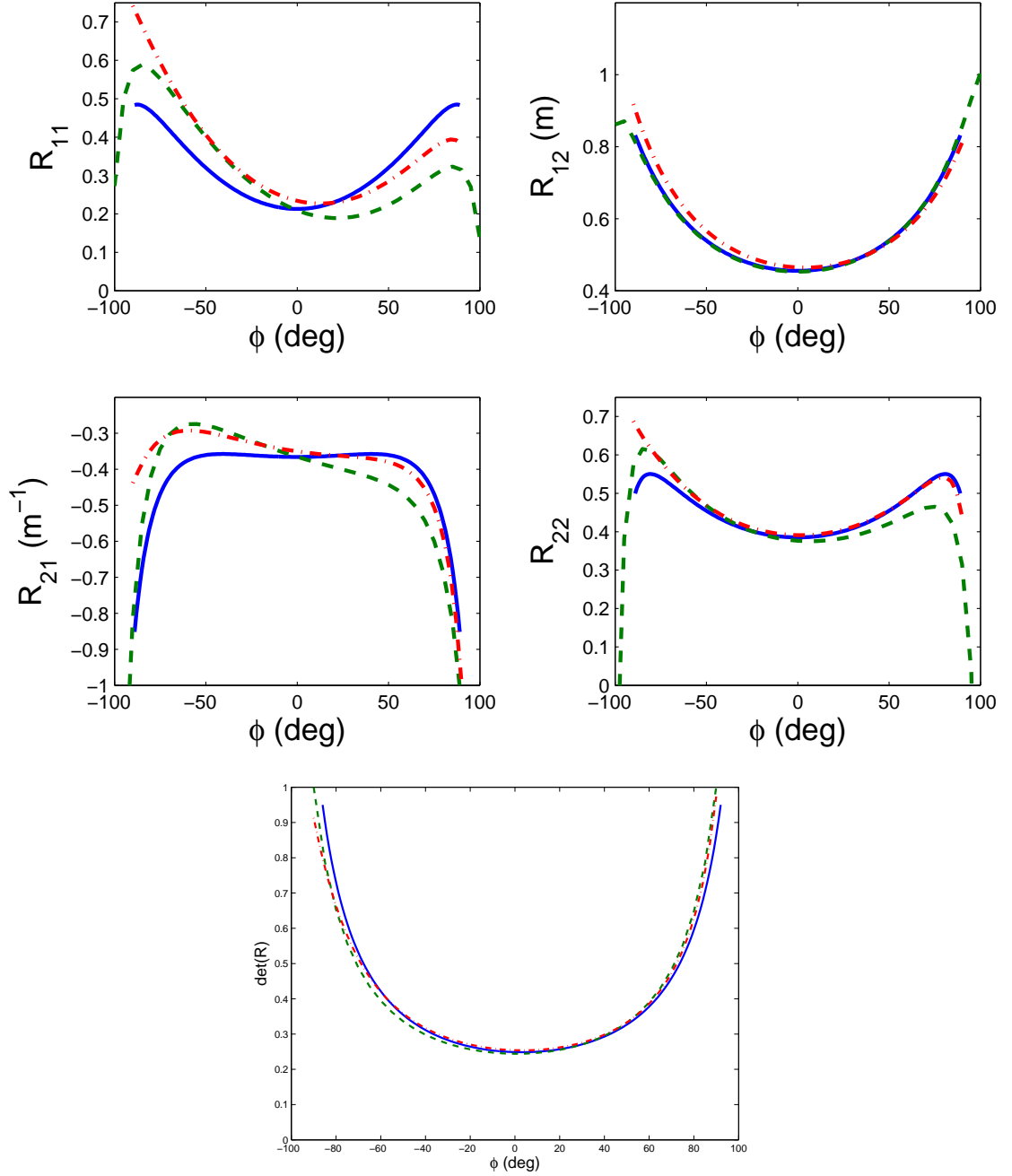


Figure 2: Transfer matrix elements and determinant dependence on the injection phase. The different curves correspond to calculations using the Chambers' model (blue solid lines), direct integration of the ODE transverse equation of motion in an rf-structure (red dashed lines) and ELEGANT simulations using an axial field of the form $E_z(z, r = 0) = E_0 \cos(kz)$ (dashed green lines).

coordinate $(x, x') = (0, 1)$ and $(0, 1)$. The obtained coordinate downstream of the cavity directly provide the element of the 2×2 transfer matrix.

2 Experimental method

The technique used to infer the transfer matrix is based on a “difference orbit” method. We use a pair of steerers to impress a known orbit perturbation upstream of the cavity. The orbit response to the perturbation, is recorded downstream of the cavity using electromagnetic beam position monitors (BPMs). Thus the orbit perturbation $\mathbf{x}_0 \doteq {}^t(x_0, x'_0)$ and associated response $\mathbf{x}_r \doteq {}^t(x_r, x'_r)$, are related accordingly to

$$\mathbf{x}_r = R\mathbf{x}_0, \quad (2)$$

where R stands for the transfer matrix between the points 0 and r . Mathematically, one needs a minimum set of four perturbations to compute the four elements of the matrix R . Practically, we impress a set of N perturbations to a “reference orbit” $\mathbf{x}_{0,0}$, $[\delta\mathbf{x}_{0,i}]_{i=1\dots N} = \mathbf{x}_{0,i} - \mathbf{x}_{0,0}$, the corresponding (measured) response $[\delta\mathbf{x}_{r,i}]_{i=1\dots N} = \mathbf{x}_{r,i} - \mathbf{x}_{r,0}$ can be casted into the system of equation:

$$\mathbf{r} \doteq \begin{bmatrix} \frac{\delta x_{r,1}}{\sigma_x} \\ \frac{\delta x_{r,2}}{\sigma_x} \\ \vdots \\ \frac{\delta x_{r,N}}{\sigma_x} \end{bmatrix} = \begin{bmatrix} \frac{\delta x_{0,1}}{\sigma_x} & \frac{\delta x'_{0,1}}{\sigma_{x'}} \\ \frac{\delta x_{0,2}}{\sigma_x} & \frac{\delta x'_{0,2}}{\sigma_x} \\ \vdots & \vdots \\ \frac{\delta x_{0,N}}{\sigma_x} & \frac{\delta x'_{0,N}}{\sigma_x} \end{bmatrix} \begin{bmatrix} r_{11} \\ r_{12} \end{bmatrix}, \quad (3)$$

and,

$$\mathbf{r}' \doteq \begin{bmatrix} \frac{\delta x'_{r,1}}{\sigma_{x'}} \\ \frac{\delta x'_{r,2}}{\sigma_{x'}} \\ \vdots \\ \frac{\delta x'_{r,N}}{\sigma_{x'}} \end{bmatrix} = \begin{bmatrix} \frac{\delta x_{0,1}}{\sigma_{x'}} & \frac{\delta x'_{0,1}}{\sigma_{x'}} \\ \frac{\delta x_{0,2}}{\sigma_{x'}} & \frac{\delta x'_{0,2}}{\sigma_{x'}} \\ \vdots & \vdots \\ \frac{\delta x_{0,N}}{\sigma_{x'}} & \frac{\delta x'_{0,N}}{\sigma_{x'}} \end{bmatrix} \begin{bmatrix} r_{21} \\ r_{22} \end{bmatrix}, \quad (4)$$

The two above systems of equation can be inverted using a least square method:

$$\begin{bmatrix} r_{11} \\ r_{12} \end{bmatrix} = [({}^t\tilde{\mathcal{P}}\tilde{\mathcal{P}})^{-1} {}^t\tilde{\mathcal{P}}]\tilde{\mathbf{r}}, \text{ and } \begin{bmatrix} r_{21} \\ r_{22} \end{bmatrix} = [({}^t\tilde{\mathcal{P}}'\tilde{\mathcal{P}}')^{-1} {}^t\tilde{\mathcal{P}}']\tilde{\mathbf{r}}'. \quad (5)$$

The error on the computed transfer matrix elements are then obtained by taking the square root of the diagonal elements of the so-called curvature matrix (${}^t\tilde{\mathcal{P}}\tilde{\mathcal{P}}$). The thereby calculated errors comes from the uncertainty on the beam position read by the BPMs, σ_{BPM} .

To account for the error coming from the uncertainty on the steerer calibration, we used a Monte-Carlo simulation. By assuming a 15% uncertainties on the steerer calibration (resulting from several calibrations of the steerers), the data reduction is done for 50 sets of steerers settings randomly generated from a Gaussian distribution with mean set to the steerer nominal set point and with a variance of 15% of its mean. The uncertainty $\sigma_{STEERER}$ coming from the steerer strength uncertainty is then obtained by computing the variance on the 50 sets of computed transfer matrix element. Finally the total error on the computed transfer matrix elements is calculated by adding quadratically the two contributions σ_{BPM} and $\sigma_{STEERER}$.

3 Experimental setup

The orbit perturbations are impressed by the mean of two pairs of horizontal and vertical steerers located upstream from the TESLA-cavity (S1 and S2 in Figure 3). The resulting orbit change downstream of the cavity are measured using electromagnetic beam position monitors (BPM's) (BPM1, BPM2 in Figure 3). The beam was first centered on the cavity axis by properly tuning the strength of the steerer S1 and S2. After centering a change of $\pm 30^\circ$ in rf-phase and 15% in accelerating gradient induced a maximum position change downstream from the cavity of $500 \mu\text{m}$ (see Figure 4). The thereby devised steerers setting results in an orbit launch which we henceforth refer to as the

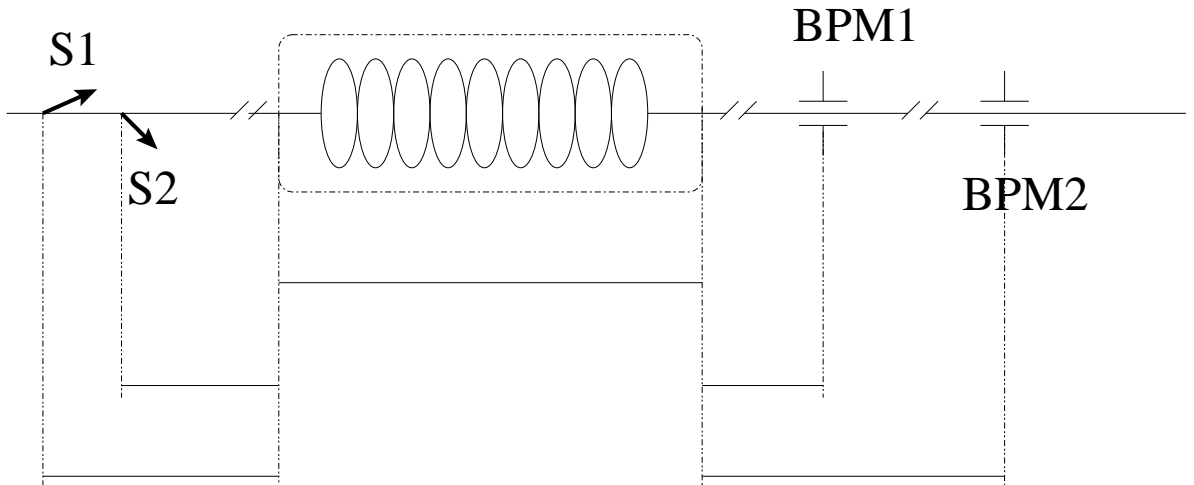


Figure 3: Experimental set-up relevant to the measurement of the TESLA-cavity transfer matrix. S1 and S2 represent the locations of the two steerers pair, and BPM1 and BPM2 the locations of the two electromagnetic beam position monitor.

“reference orbit”. Under the thin length approximation the steerers are well approximated by an angular kick model. Thus given the angular kick imparted by S1 and S2 (respectively $\delta x'_{S1}$ and $\delta x'_{S2}$), the corresponding position and angle changes at the cavity entrance and with respect to the reference orbit launch are:

$$\begin{aligned}\delta x_0 &= \delta x'_{S1} L_{S1 \rightarrow 0} + \delta x'_{S2} L_{S2 \rightarrow 0} \\ \delta x'_0 &= \delta x'_{S1} + \delta x'_{S2},\end{aligned}\tag{6}$$

wherein $L_{a \rightarrow b}$ denotes the distance between points a and b . Similarly given the positions changes at BPM1 and BPM2 (respectively δx_{BPM1} and δx_{BPM2}), the corresponding position and angle changes at the cavity exit are given by:

$$\begin{aligned}\delta x_r &= \delta x_{BPM2} - \delta x'_r L_{r \rightarrow BPM2} \\ \delta x'_r &= \frac{\delta x_{BPM2} - \delta x_{BPM1}}{L_{BPM1 \rightarrow BPM2}}.\end{aligned}\tag{7}$$

The latter Eq. 6, 7 provide all the information needed for computing the systems given in Eq. (5).

The steerers magnetic field has been measured and we report an example of such a measurement in Figures 5 and 6.

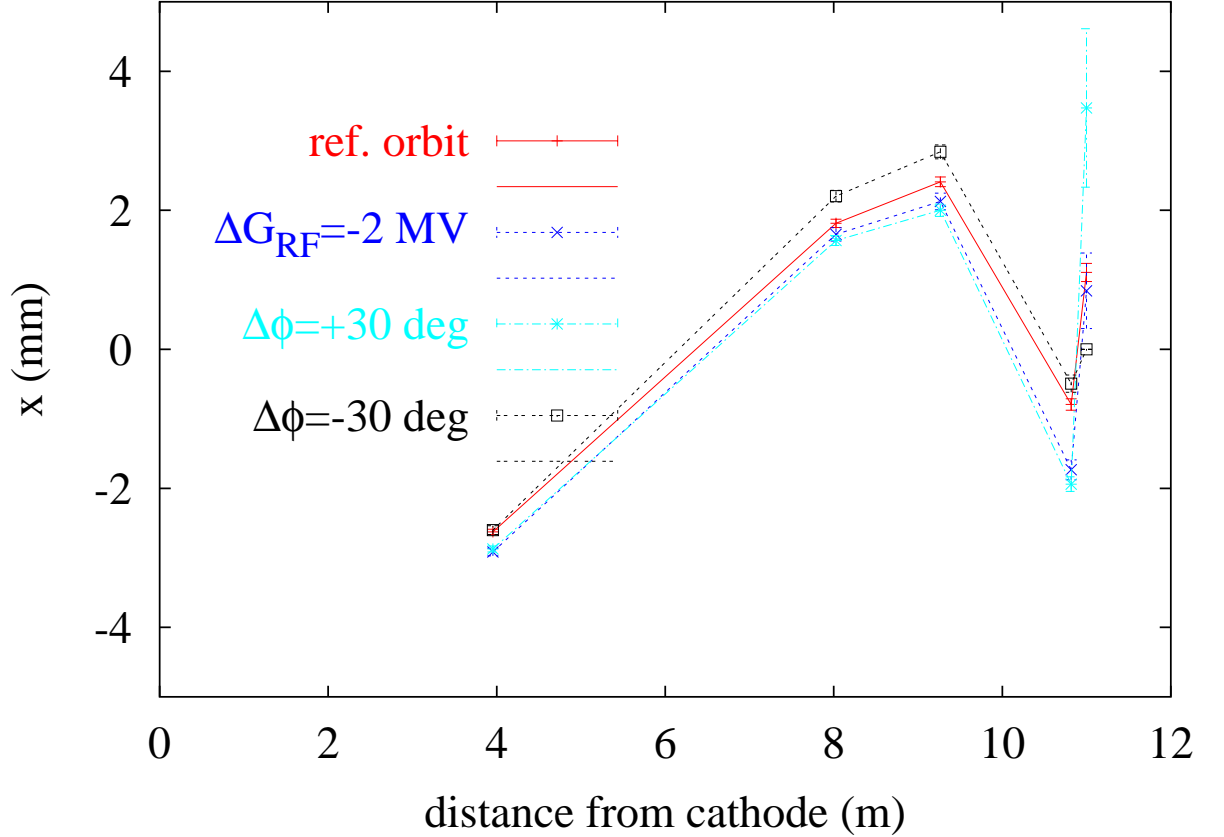


Figure 4: Orbit variation along the beamline downstream from the cavity for different settings of the cavity phase and gradient set points. The last position measurement at $z \simeq 11$ m is performed downstream of the spectrometer and is thus representative of the beam momentum.

Saturation effects on the B versus I curve can be observed when the steerer is operated at the maximum allowed excitation current (5 A) and the on-set of the saturation starts to be visible at 2.5 A; these saturations effects are not important for the experiment discussed in this Note: the typical maximum excitation current is below 2 A.

The hysteresis curve of the steerers have been measured (see Fig.6). After various tests, we followed the following procedure to “degauss” the steerers:

1. cycle the steerer using an oscillating current excitation with exponential decay,

$$I = I_0 \cos(\omega t) \exp(-t/\tau)$$
2. set the steerer to its maximum positive value,
3. decrease the current to the desired set point.

The step (2) of the above procedure implies we operate the steerer in the upper part of the hysteresis loop thereby insuring the B-field dependence on the current is linear especially when operating with excitation current within ± 2 A.

The measured B-field profile versus z can be fitted with the analytical approximation for the field profile resulting from coils:

$$B(z) = B_0 + \frac{\hat{B}}{\cosh(z/a)}, \quad (8)$$

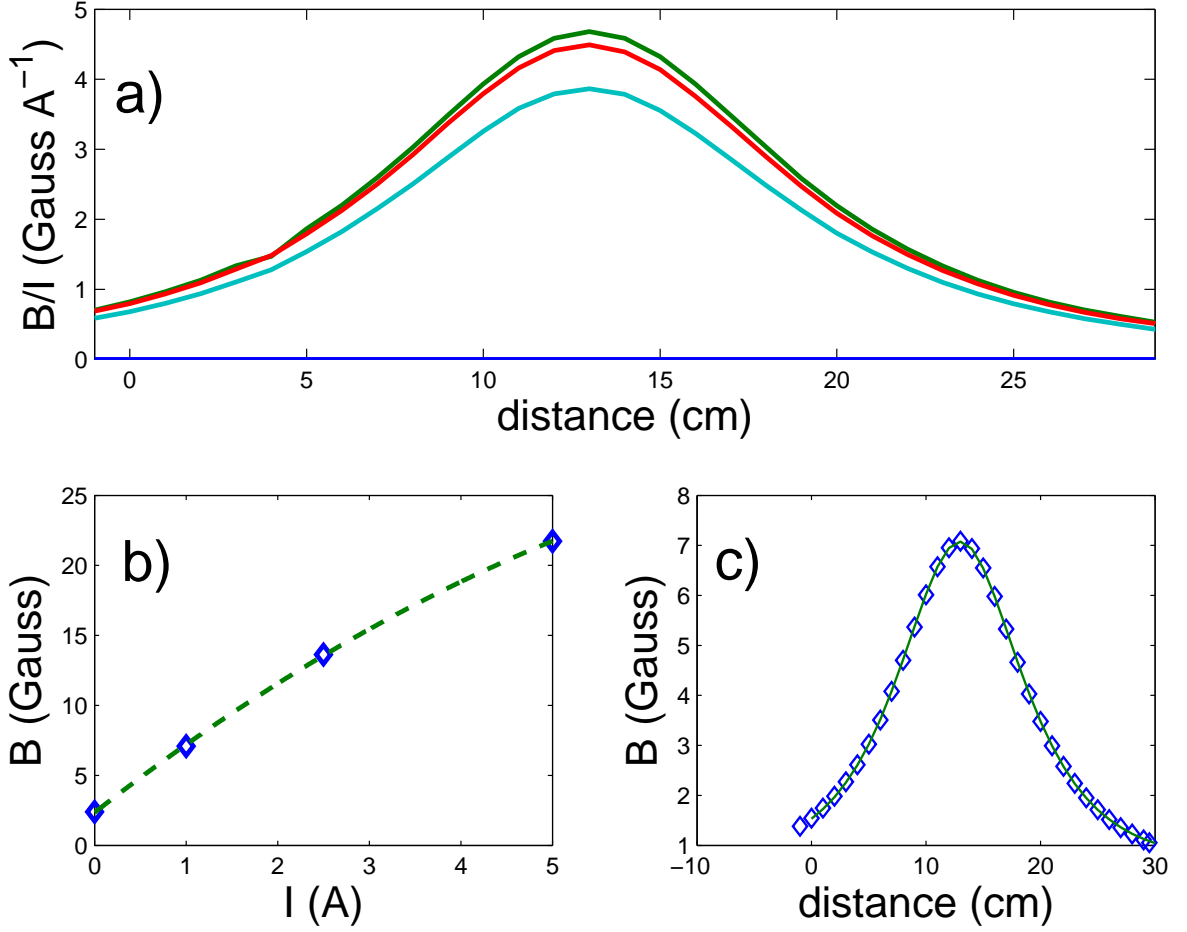


Figure 5: Measured $B_y(z, x = 0, y = 0)$ field profile for the first steerer for different excitation currents a). The corresponding field maximum value versus excitation current is shown in plot b). The measured field profile (diamonds) fitted with Eq. (8) (solid line) is presented in plot c) for an excitation current of 1 A.

where \hat{B} , a and B_0 are some free parameters that need to be extracted from the measurement. A fit of the measurement is also presented in Figure 5 and the resulting relevant values are $a = 4.82$ cm and $\hat{B} = 4.28$ G for a 1 A excitation current. The magnetic field offset is found to be $B_0 = 0.53$ G, a value consistent with the Earth magnetic field. The advantage in using Eq.(8) for modeling the field is that the kick imparted by the steerer can be then estimated analytically from:

$$\frac{dx'}{dI} = \frac{e \int_{-\infty}^{+\infty} B(z) dz}{p_{\parallel}} = \frac{e}{p_{\parallel}} \left[2a\hat{B} \arctan(\tanh(z/(2a))) \right]_{-\infty}^{+\infty} = \frac{e}{p_{\parallel}} \pi a \hat{B}, \quad (9)$$

that is in practical units:

$$\frac{dx'}{dI} [\text{rad/A}] = \frac{1.9436 \times 10^4}{p_{\parallel} [\text{eV}]} \quad (10)$$

Taking into account the length between the steerer (here we consider HTB9C) and the first BPM,

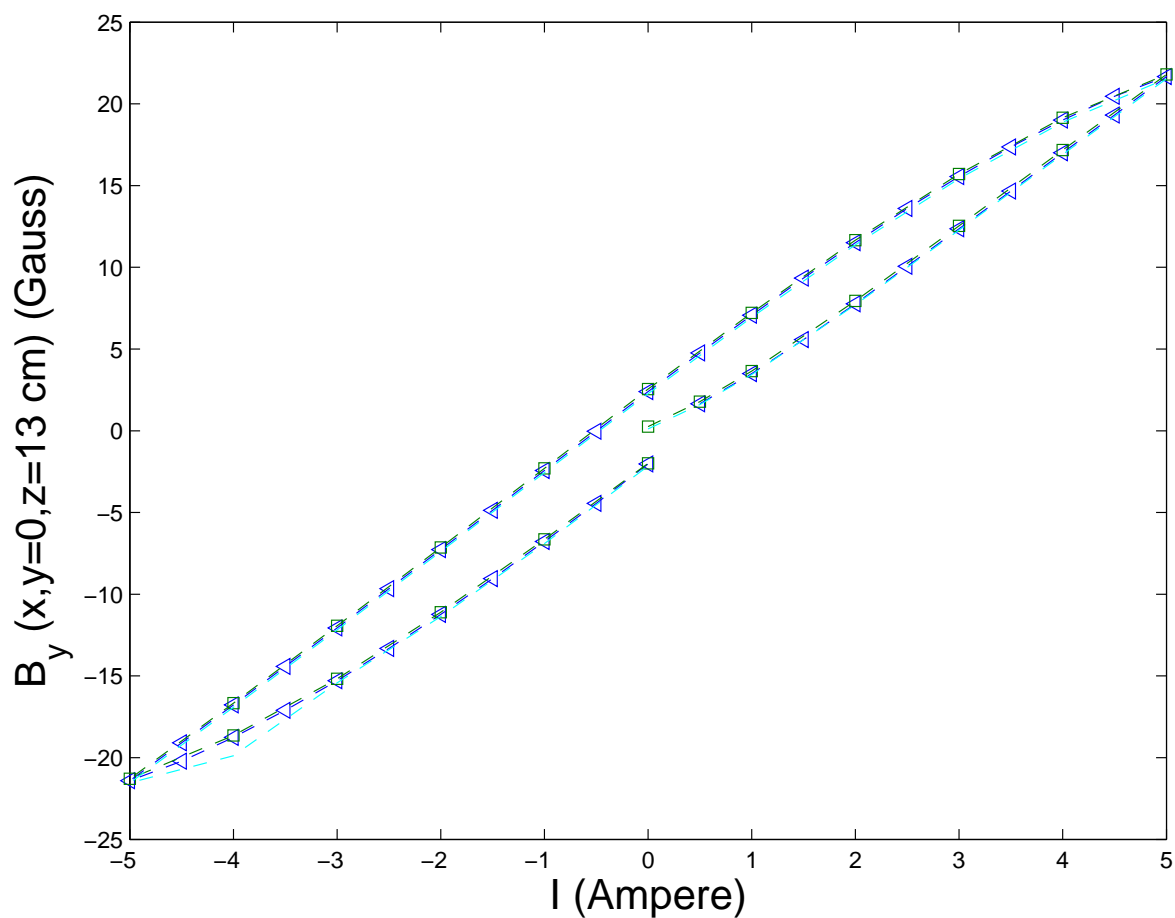


Figure 6: Measured $B_y(z \simeq 13 \text{ cm}, x = 0, y = 0)$ field hysteresis curve

one finally gets:

$$p_{\parallel} c[\text{eV}] = \frac{6.1806 \times 10^4}{(dx)/(dI)}, \quad (11)$$

wherein $(dx)/(dI)$ is in units of $\text{m}\cdot\text{A}^{-1}$.

4 Results obtained so far

A series of measurement were repeated in 2003, on Feb 6, Feb 11, and Feb 13. The measurements were reproducible and yield the transfer matrix elements presented in Fig. 7. We generally observed a strong disagreement between experiment and theoretical calculations for the first row of the matrix (R11 and R12). The second row is in better agreement. The determinant, within the errorbars, exhibits the behavior expected from adiabatic damping.

5 Future work

To date the agreement between the experimental measurement and numerical calculated transfer matrix element is far from satisfactory. Work is on going to try to resolve the observed disagreement. On the experimental point-of-view, the procedure we use to align the beam is being refined: we are plan to align the beam on the cavity axis by minimizing the detected high order mode (HOM) power associated to long range dipole mode wake-field [5]. The numerical model also need to be refined, e.g. by including possible effects from the HOM and input couplers [6].

References

- [1] E. Chambers, Stanford High Energy Physics report (1965) (unpublished)
- [2] J. Rosenzweig, L. Serafini, *Phys. Rev. E* **47**, 2031 (1994)
- [3] R. Tikhoplav, et al., presented at LINAC 2004 Lübeck Germany , 16-20 Aug 2004. Fermilab preprint fermilab-conf-04-191-ad (2004)
- [4] S. Fartoukh, DESY report TESLA 98-01 (1998)
- [5] N. Baboi, et al., presented at LINAC 2004 Lübeck Germany August 2004
- [6] P. Piot, M. Dohlus, K. Flöttmann, and S. G. Wipf, in preparation

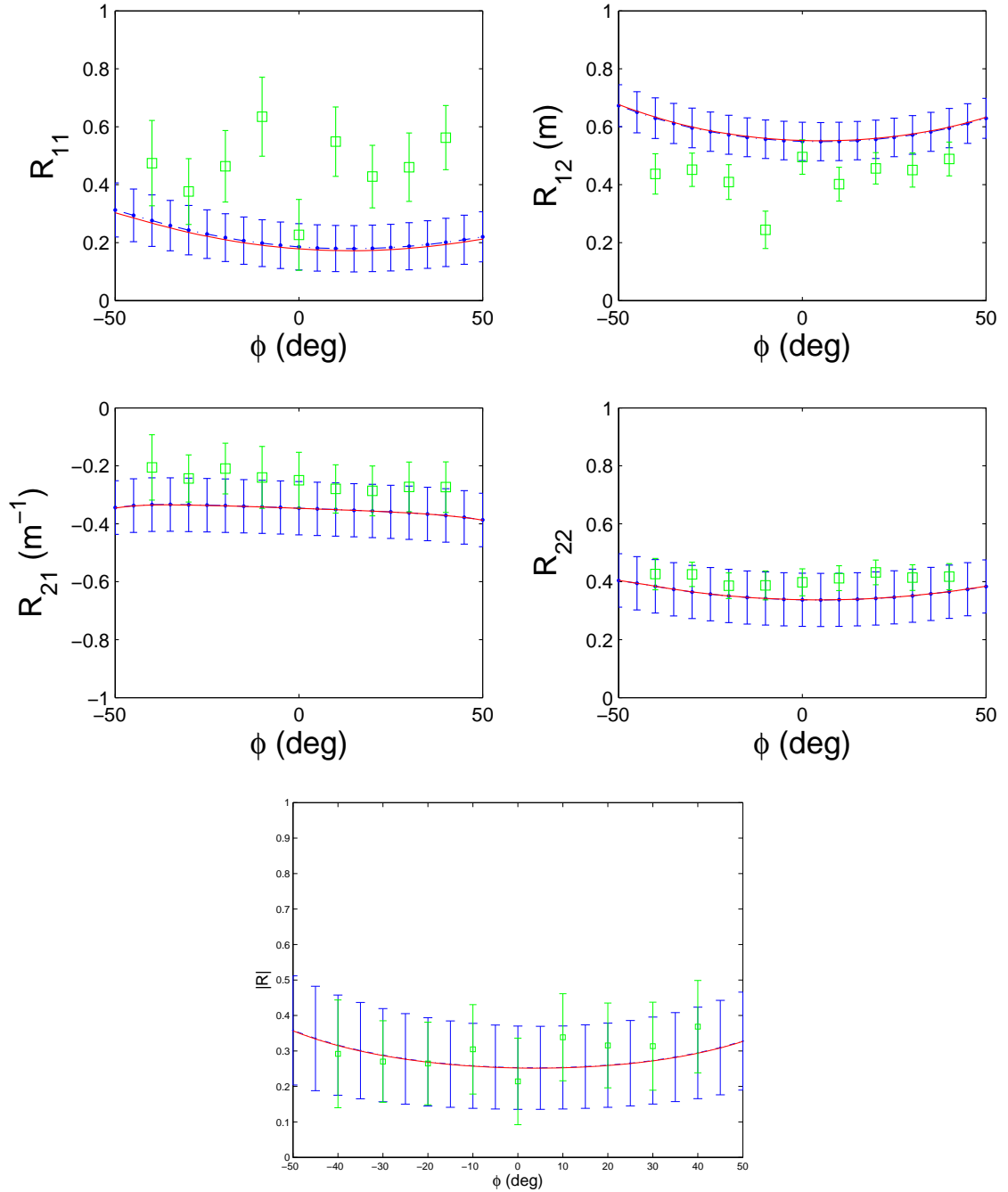


Figure 7: Experimental measurement of the transfer matrix element and inferred determinant.